Passive antenna characterization through impedance correlations in a diffuse field

Meriem Tamart, Julien de Rosny, Elodie Richalot

Passive antenna characterization through impedance correlations in a diffuse field

Meriem Tamart, Julien de Rosny, *Member, IEEE*, and Elodie Richalot, *Member, IEEE*

***Abstract*—Ambient noise correlations allow the passive recovery of Green's functions between two probes. Recently, the same approach has been applied to electromagnetism, but by correlating diffuse fields in mode stirred chambers. Until now, only correlation of S-parameters has been studied. However, it has very recently been shown that the result can be difficult to interpret. To overcome this limitation, a new approach is proposed in this paper to directly estimate the self and mutual impedances of two coupled antennas from impedance correlations. The theoretical developments presented are validated experimentally in a reverberation chamber excited by a single antenna where mechanical and source stirring techniques are combined to generate a sufficiently diffuse field environment. It is shown, with antennas of different properties, that this approach allows to reconstruct with a good accuracy the complex impedance matrix between two receiving antennas as well as the transmission coefficient between them. The extracted gain pattern, in good agreement with that measured in an anechoic chamber, shows the good sensitivity of the proposed passive characterization technique.**

***Index Terms*—antenna coupling, cross-correlation, passive antenna measurement, reverberation chamber**

I. Introduction

SINCE the pioneer work of Weaver and Lobkis in 2001 based on the fluctuation-dissipation theorem [1], [2], cross-correlation techniques have been used in numerous physics domains to retrieve, from the recording of the diffuse field generated by noise sources, the Green's function between two passive and non-invasive point-like sensors, as if a pulse were emitted by one of the sensors. The convergence of the cross-correlation of the field requires the equipartition of the noise field. This approach has been used to gain information about the propagation medium, as in geophysics where the elastic response of Earth has been investigated [3] or for passive structural health monitoring with the detection of defect appearance [4], [5]. Information about the sensors themselves can also be extracted as with their localization [6].

A first experimental demonstration of electromagnetic Green's function retrieval in the microwave range has been performed in anechoic and reverberant cavities by computing the average cross-correlation of noise signals generated by a wideband diffuse thermal radiation, and the ability to detect and locate a scattering object solely using this thermal ambient has been demonstrated [7]. To increase the field intensity, an emitting antenna has then been used as a source; the equipartitioned field has been obtained while performing measurement within a reverberation chamber (RC) inducing field multiple scattering for different cavity configurations thanks to the mode-stirrer rotation [8] or a programmable metasurface [9]. The influence of antenna properties on the cross-correlation result has been highlighted using an antenna and an electro-optical probe as sensors [8]. Indeed, whereas the time domain cross-correlation converges towards the sum of the anticausal and causal Green's functions with noninvasive probes, only the anticausal Green's function can be retrieved when the electro-optical probe is used along with an absorbing antenna, as a consequence of the incoming energy absorption by the matched antenna.

The underlying principle beyond the passive estimation of the Green's function from noise correlation can be related to the thermodynamic equilibrium. In 1946, Dick [10] predicted that the power spectral density (PSD), i.e. the Fourier transform of the autocorrelation, induced on a matched antenna by the radiations generated by the walls of a black body cavity at a given temperature is equal to the autocorrelation of Johnson's noise generated by the matched load at the same temperature. Later, this equivalence principle was generalized to the cross power spectral density (CSD) based either on the fluctuation dissipation theorem [11] or on Thevenin's theorem [12]. In [8], this principle has been applied to RCs based on the heuristic assumption that the diffuse field generated in such a room is equivalent to the thermal field generated by the surfaces of a virtual black body at the boundary of the reflective cavity. Only recently [13], it was rigorously shown based on the unitary of the scattering matrix (S), that the CSD of the S parameters between one transmit antenna and 2 receive antennas, i.e. $C_{S12}(\omega) \equiv \langle S_{1Tx}(\omega) S^*_{2Tx}(\omega) \rangle$, converges toward

$$C_{S12}(\omega) \approx -\eta \left\langle S^*_{21}(\omega).S_{11}(\omega) + S_{12}(\omega).S^*_{22}(\omega) \right\rangle , \qquad (1)$$

where η is the ratio of the number of antenna ports over the number of all ports including virtual ones which account for room losses. Symbol $\langle \cdot \rangle$ indicates an averaging over all measurement configurations. However, first this expression is difficult to exploit in order to passively estimate the coupling parameters S_{12} and S_{21} because it also depends on the unknown factor η and the reflection parameters S_{11} and S_{22}, and second it is only valid for lossless antennas.

For this reason, we propose here an alternative approach based on the cross-spectral density between mutual impedances $C_{Z12}(\omega) \equiv \langle Z_{1Tx}(\omega).Z^*_{2Tx}(\omega) \rangle$. We show it converges directly toward the radiation impedance between both receiving antennas Z_{12} and some simple properties of the

Manuscript received December XX, 2022; revised XX, 2022

M. Tamart and E. Richalot are with Univ Gustave Eiffel, CNRS, ESYCOM, F-77454 Marne-la-Vallée, France (e-mail: elodie.richalot-taisne@univ-eiffel.fr).

J. de Rosny is with Institut Langevin, ESPCI Paris, Université PSL, CNRS, 75005 Paris, France (e-mail: julien.derosny@espci.fr).

RC and the transmitter. As the self-impedances Z_{11} and Z_{22} can be retrieved through the calculation of the autocorrelation, the whole Z-matrix between both antennas can be estimated allowing a complete passive characterization of two coupled antennas. The knowledge of the impedance matrix can then be exploited to extract other parameters of interest such as antenna reflection coefficients or radiation pattern. This correlation approach would thus permit to characterize antennas and the coupling between them while keeping antennas under test in their receiving mode that is in particular mandatory for small integrated antennas that cannot be turned into their emitting mode.

A first demonstration of the capability to retrieve passively within a reverberation chamber the mutual impedance between two antennas had been presented in a previous paper [14], but without calculating the proportionality coefficient between both entities; as a consequence, only normalized results were presented and, as this coefficient varies versus frequency, a distortion of the time response was observed. The theoretical developments presented for the first time in this paper permit to determine the real amplitudes of the three impedances. Similarly to [13], the proportionality factor accounts for the cavity losses in a simple way through the cavity damping coefficient. Besides, our impedance approach allows managing the antenna's losses through the antenna efficiency, whereas only lossless antennas had been considered until now.

This paper first of all presents in Section II the theoretical developments leading, in the case of two coupled antennas placed within a mode stirred RC excited by an antenna, to the relationships between, on one hand, the CSD between Z_{1Tx} and Z_{2Tx} and the real part of mutual impedance Z_{12} between both receiving antennas, and on the other hand between the PSD and the real parts of their self impedances. These theoretical formulas are then validated in Section III while using, as receiving antennas, two facing horn antennas of different characteristics. In Section V-C, we will discuss how to estimate the impedance correlation using high impedance loads. It is also shown that, besides the real parts of the impedances, their imaginary parts can also be reconstructed after a suited post-processing step and, once the total complex impedance matrix is known, the transmission coefficient can also be passively estimated. The robustness of our method is also tested for two coupled receiving antennas of different natures, indeed a horn antenna and a slot antenna. Section IV is dedicated to the application of the correlation technique to estimate in a passive way the gain pattern of an antenna. After discussions on the measurement conditions, a conclusion ends this paper.

II. Theory

The equivalent system of the antenna network considered here is depicted in Fig. 1. In this section, all the quantities are considered in the frequency domain and their frequency dependence are implicit. There is one transmitting antenna of self impedance Z_{Tx} excited by a current generator of intensity I_{Tx}; this antenna is considered to be far enough from the two receiving antennas so that its radiation properties are not modified by their presence, whereas the two receiving antennas are coupled to each other. The Tx-antenna induces an electromotive force e_1 (resp. e_2) at the terminal of receiving antenna 1 (resp. 2). The voltage and current at the antenna port of antenna 1 (resp. 2) are U_1 and I_1 (resp. U_2 and I_2). The electromotive forces are related to the currents by the generalized Ohm's law

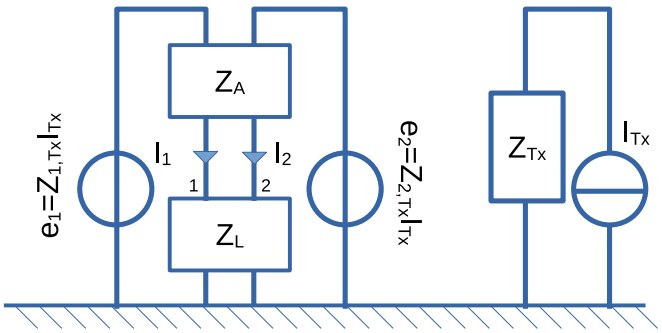

Fig. 1. Equivalent linear system of the interaction between one transmitting antenna (Tx) and two coupled receiving antennas labeled 1 and 2.

$$\mathbf{e} = (\underbrace{\mathbf{Z}_L + \mathbf{Z}_A}_{\mathbf{Z_T}})\mathbf{I},$$

where $\mathbf{e} = (e_1, e_2)^t$ and $\mathbf{I} = (I_1, I_2)^t$. The self and cross interactions between antennas 1 and 2 is modeled by the 2-by-2-element impedance matrix $\mathbf{Z}_A$. The matrix $\mathbf{Z}_L$ is a generalization of the load impedance to a network system. The correlations between the electromotive forces can be expressed in terms of $\langle \mathbf{I}\mathbf{e}^H \rangle$ (subscript H stands for the transpose conjugate)

$$\left\langle \begin{pmatrix} e_1 \\ e_2 \end{pmatrix} (e_1^*, e_2^*) \right\rangle = \begin{pmatrix} \langle e_1 e_1^* \rangle & \langle e_1 e_2^* \rangle \\ \langle e_2 e_1^* \rangle & \langle e_2 e_2^* \rangle \end{pmatrix} = \mathbf{Z_T} \left\langle \begin{pmatrix} I_1 \\ I_2 \end{pmatrix} (e_1^*, e_2^*) \right\rangle. \quad (2)$$

The network of the two receiving antennas is matched when $\mathbf{Z}_L$ is equal to $\mathbf{Z}_A^H$ [15]. In such a case, the impedance matrix $\mathbf{Z}_T$ is Hermitian. As a consequence, it can be diagonalized, i.e., it exists two orthonormal eigenstates ($\mathbf{u}_1$ and $\mathbf{u}_2$) and two complex eigenvalues (z_T^1 and z_T^2) such as

$$\mathbf{Z}_T \mathbf{u}_{1,2} = z_T^{1,2} \mathbf{u}_{1,2}. \quad (3)$$

Introducing the projection matrix such as $\mathcal{P} = (\mathbf{u}_1, \mathbf{u}_2)$, $\langle \mathbf{I}\mathbf{e}^H \rangle$ can be expressed in terms of eigenstates

$$\langle \mathbf{I}\mathbf{e}^H \rangle = \mathcal{P} \left\langle \begin{pmatrix} I_1' \\ I_2' \end{pmatrix} (e_1'^*, e_2'^*) \right\rangle \mathcal{P}^H, \quad (4)$$

where $'$ indicates that the quantity is described on the basis of the eigenvectors. Because the antennas are perfectly matched, the system behaves as two virtual independent antennas with orthogonal radiation patterns which absorb all the incident energy. As a consequence,

$$\left\langle \begin{pmatrix} I_1' \\ I_2' \end{pmatrix} (e_1'^*, e_2'^*) \right\rangle = \begin{pmatrix} 2\langle P_1 \rangle & 0 \\ 0 & 2\langle P_2 \rangle \end{pmatrix}. \quad (5)$$

where $\langle P_1 \rangle$ and $\langle P_2 \rangle$ are the powers absorbed by each virtual antenna. As shown by Hill [16], the mean power absorbed

by a lossless single port antenna in a random diffuse and unpolarized field environment is given by

$$\langle P_1 \rangle \quad = \langle P_2 \rangle = \quad \frac{\langle \Pi \rangle \lambda^2}{8\pi}, \tag{6}$$

where Π is the power density. Combining Eqs. (2), (4), (5) and (6), it comes

$$\begin{pmatrix} \langle e_1 e_1^* \rangle & \langle e_1 e_2^* \rangle \\ \langle e_2 e_1^* \rangle & \langle e_2 e_2^* \rangle \end{pmatrix} = \frac{\langle \Pi \rangle \lambda^2}{4\pi} \left(\mathbf{Z}_A^H + \mathbf{Z}_A \right), \tag{7}$$

because $\mathcal{P}\mathcal{P}^H$is equal to the identity matrix. In average, the power density is related to the energy density W by

$$\langle \Pi \rangle = c \langle W \rangle . \tag{8}$$

with c the speed of light. At steady state regime, the power emitted by the source $\langle P_{Tx} \rangle$ is absorbed by all the dissipation processes in the chamber of volume V, i.e.,

$$\langle P_{Tx} \rangle = \langle W \rangle V \alpha, \tag{9}$$

where α the energy decay rate of the chamber. Finally, the energy emitted by the source can also be expressed in terms of the antenna efficiency η_{Tx}, the real part of the impedance $\Re(Z_{Tx})$ and the current I_{Tx},

$$P_{Tx} \quad = \quad \eta_{Tx} \Re(Z_{Tx}) \left| I_{Tx} \right|^2 . \tag{10}$$

From Eqs. (7), (8), (9) and (10) it comes

$$\left\langle \mathbf{e}\mathbf{e}^H \right\rangle \quad = \quad (\mathbf{Z}_A^H + \mathbf{Z}_A) \frac{\lambda^2 c \eta_{Tx} \Re(Z_{TxTx}) \left| I_{Tx} \right|^2}{4\pi\alpha V}. \tag{11}$$

Because the electromotive forces can be written in terms of mutual impedances ($\mathbf{e} = \left(Z_{1Tx}, Z_{2Tx} \right)^t I_{Tx}$), the correlation between the impedances of the transmitting antenna and the two receiving ones can be expressed in terms of the self and mutual impedances of antennas 1 and 2,

$$\mathbf{C}_Z^{\text{Theo}} \quad = \quad \begin{pmatrix} \langle Z_{1Tx} Z_{1Tx}^* \rangle & \langle Z_{1Tx} Z_{2Tx}^* \rangle \\ \langle Z_{2Tx} Z_{1Tx}^* \rangle & \langle Z_{2Tx} Z_{2Tx}^* \rangle \end{pmatrix} \tag{12}$$

$$= \quad (\mathbf{Z}_A^H + \mathbf{Z}_A) \frac{\lambda^2 c \eta_{Tx} \Re(Z_{TxTx})}{4\pi\alpha V}. \tag{13}$$

This expression is valid for lossless antennas. To take into account the losses, a model of Ohmic loss should be introduced. Here we assume a simple model where Ohmic losses can be isolated as an impedance in series

$$\mathbf{Z}_A \quad = \quad \mathbf{Z}_A^\Omega + \mathbf{Z}_A^R. \tag{14}$$

where $\mathbf{Z}_A^R$ is a complex matrix accounting for radiative losses and the Ohmic impedance matrix $\mathbf{Z}_A^\Omega$ is a diagonal matrix

$$\mathbf{Z}_A^\Omega = \begin{pmatrix} R_1 & 0 \\ 0 & R_2 \end{pmatrix}, \tag{15}$$

with R_1 and R_2 are the electrical resistances related to Ohm losses on antennas 1 and 2, respectively. The above formalism can be applied but with a load impedance which compensates the Ohmic losses. It is then given by

$$\mathbf{Z}_L = (\mathbf{Z}_A^R)^H - \mathbf{Z}_A^\Omega \tag{16}$$

Then Eq. (12) is still valid but $\mathbf{Z}_A$ has to be replaced by $\mathbf{Z}_A^R$. Using Eqs. (14), (15) and (12), it is straightforward to show that the CSD $\mathbf{C}_{Zi\neq j}^{\text{Theo}} = \left\langle Z_{iTx} Z_{jTx}^* \right\rangle$, is given by

$$\mathbf{C}_{Zi\neq j}^{\text{Theo}} = \frac{\lambda^2 c \eta_{\text{TxTx}} \Re(Z_{\text{TxTx}})}{2\pi\alpha V} \Re(Z_{ij}) \tag{17}$$

and the PSD $\mathbf{C}_{Zii}^{\text{Theo}} = \langle Z_{iTx} Z_{iTx}^* \rangle$, by

$$\mathbf{C}_{Zii}^{\text{Theo}} = \frac{\lambda^2 \eta_{\text{Tx}} c \eta_i \Re(Z_{\text{TxTx}})}{2\pi\alpha V} \Re(Z_{ii}), \tag{18}$$

where $\eta_i = R_i / \Re(Z_{ii})$ is the radiation efficiency of antenna i.

It has to be noticed that the proportionality coefficients in Eqs. (17) and (18), presented for the first time in this paper, vary with respect to the frequency, so that the impedance cannot be retrieved with accuracy if they are not accounted for.

III. Experimental Validation

A. Measurement Setup

All experiments are performed within the ESYCOM RC of dimensions $2.95 \times 2.75 \times 2.35$ m^3 (Fig. 2), whose lowest usable frequency is estimated to be 400 MHz. It is equipped with a Z-fold mechanical stirrer and $N_{\text{mech}} = 60$ equally-spaced positions are considered over a revolution. The two antennas under test (AUTs) are double-ridged horn antennas, the first one, labelled "1" in the following, of 1GHz-18GHz bandwidth (Schwarzbeck BBHA 9120B), and the second one, labelled "2", of 1GHz-18GHz bandwidth (A-INFO JXTXLB-10180). Both AUTs are facing each other, separated by a distance $d = 50\ cm$. They are placed within the RC working volume in such orientation so that they do not face flat walls with normal incidence, in order to avoid unstirred paths in the RC. The source antenna, named "Tx" thereafter, is a horn antenna identical to AUT1, oriented towards the mechanical stirrer and positioned on a vertically-rotating structure in order to perform source stirring over $N_{\text{src}} = 11$ positions; indeed, the source antenna orientation in regard to the floor plane varies from $-35°$ to $+35°$ with an angular step of $7°$. Each AUT is linked, through a 50 cm-long coaxial cable, to a remotely-controlled mechanical RF switch, in order to be connected either to a VNA or to an open-circuit (OC) load impedance (see Fig. 3). It has to be underlined that, in an application case, as with embedded antennas, the measurement has to be performed by the receiving antenna connected to a high impedance probe. However, here for convenience, the impedances Z_{1Tx} and Z_{2Tx} are measured with a VNA. Of course, using a VNA with 50Ω ports is not interesting for practical applications. Nevertheless, it permits in a validation step a complete characterization of the studied system. Scattering parameters measurements are carried out over the 1 to 5 GHz frequency range (20001 frequency points with an IF BW of 10 kHz) with a Rohde & Schwarz ZNB20 4-port VNA calibrated at the end of both cables connected to both switches (reference planes indicated in Fig. 3). The efficiencies of the used antennas have been previously estimated within the same RC at the same frequencies following the approach described in [17]: in order to avoid any bias due to unstirred paths, measurements

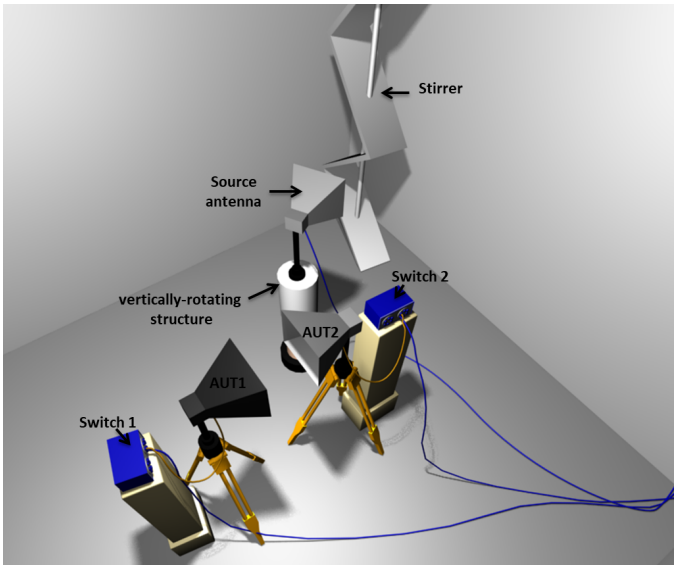

Fig. 2. Schematic of the measurement setup within the RC, with the excitation antenna pointing towards the mode stirrer and of varying azimuthal angle, and two facing antennas in reception connected to switches.

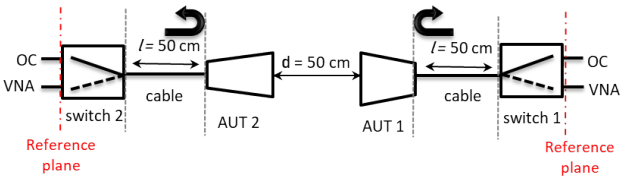

Fig. 3. Schematic of the measurement setup and reference planes considered for measurements.

have been performed over a stirrer rotation (60 positions) for several orientations of the antenna pointing towards the mode-stirrer and the one placed within the RC working volume (11 orientations for both antennas). The mean efficiencies over the frequency range are of 0.916 for AUT1 and 0.822 for AUT2.

Three configurations are successively measured:

- Config$_{ref}$: Both AUTs are connected to the VNA. This configuration will serve as a reference to directly measure Z_{12}, Z_{11} and Z_{22}, and compare them to the reconstructed ones;
- Config$_1$: The AUT1 is connected to the VNA while the AUT2 is connected to the OC. $Z_{1\mathrm{Tx}}$ will be computed then used in correlation calculation;
- Config$_2$: The AUT2 is connected to the VNA while the AUT1 is connected to the OC. $Z_{2\mathrm{Tx}}$ will be computed then used in correlation calculation.

B. Theory validation

We will first of all verify that, according to Eqs. (17) and (18), it is possible to retrieve the real parts of $Z_{ii}(f)$ and $Z_{ij}(f)$ through the correlation of the measured impedances $Z_{1Tx}(f)$ and $Z_{2Tx}(f)$.

The real part of the mutual impedance $Z_{12}(f)$ calculated directly from the measured S-parameters in Config$_{ref}$ (named $Z_{R12}(f)$ thereafter) is compared to $Z_{R12}^{corr}(f)$. The later is

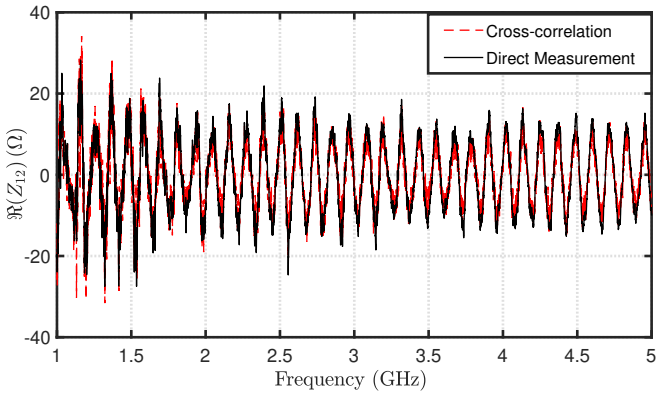

Fig. 4. Real part of Z_{12} obtained by a direct measurement between both horn antennas or through CSD between impedances Z_{1Tx} and Z_{2Tx} as a function of frequency.

estimated from the CSD between $Z_{1Tx}(f)$ of Config$_1$ and $Z_{2Tx}(f)$ of Config$_2$ in Fig. 4. Compared to previous works [14], notice that, thanks to the knowledge of the proportionality factor given in Eq. (17), amplitudes are not normalized here. A very good agreement is observed between measurement and theory. The time-domain variation of the real part of Z_{12} is then computed thanks to an inverse Fourier transform of the CSD. The result is presented in Fig. 5. As $Z_{R12}^{corr}(f)$ is real and $C_{Z12}(f)$ is almost real (in accordance with Eq. (17)), the time variations of $Z_{R12}(t)$ and $Z_{R12}^{corr}(t)$ are symmetrical with respect to $t = 0$. Consequently, both causal and anti-causal responses are exhibited.

Fig. 5 shows the appearance of a high transmission peak having a maximum value at $t = 8.58\ ns$, corresponding to the direct path between both calibration planes after the switches connected to both AUTs (see Fig. 3). This transmission time is in agreement with the propagation time over the air (over the distance $d = 50\ cm$) then within the antennas (over 30 cm in AUT1 and 20 cm in AUT2 between antenna opening and SMA access) and both cables of length $l = 50\ cm$. A second smaller peak is observed 5 ns after the larger one, this time corresponding to twice the signal traveling time along the 50 cm-long cable that connects the switch to the antenna access. This second peak is thus due to a reflection phenomenon at the connection discontinuities between the cables and the switchs or the AUTs.

To experimentally validate (18), the PSD C_{Z11} and C_{Z22} measured in Config$_1$ and Config$_2$ are calculated and lead to the estimation of the real parts of Z_{11} (named Z_{R11}^{corr}) and Z_{22} (named Z_{R22}^{corr}), respectively. Note that the considered efficiency includes antenna Ohmic losses (through antenna radiation efficiency) as well as the attenuation in the 50 cm-long connection cable and the switch (between the antenna connector and the reference plane) ; these losses have been previously measured. The time and frequency variations of these estimated impedances are compared to the real parts of Z_{11} and Z_{22} obtained by a direct measurement in Config$_{ref}$ (Z_{R11} and Z_{R22}) in Figs. 6 and 7. To estimate the imaginary part of Z_{12}, we perform a time folding of the negative times of $Z_{R12}^{corr}(t)$ toward the positive time. The new time dependent

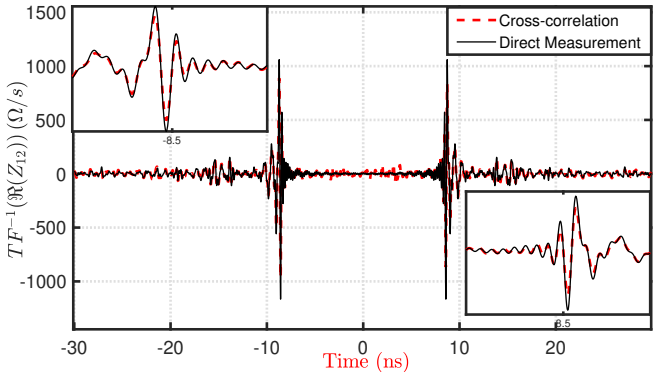

Fig. 5. Inverse Fourier Transform of the real part of Z_{12} obtained by a direct measurement between both horn antennas or through CSD between impedances Z_{1Tx} and Z_{2Tx} as a function of time. Insets present zoom on the first peak for negative and positive times.

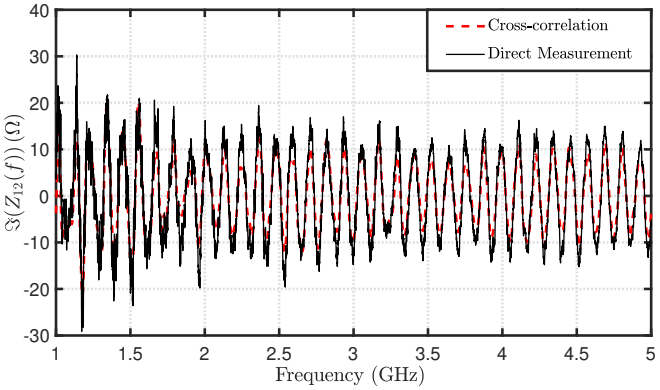

Fig. 8. Imaginary part of Z_{12} obtained by a direct measurement between both horn antennas or through CSD between Z_{1Tx} and Z_{2Tx} as a function of frequency.

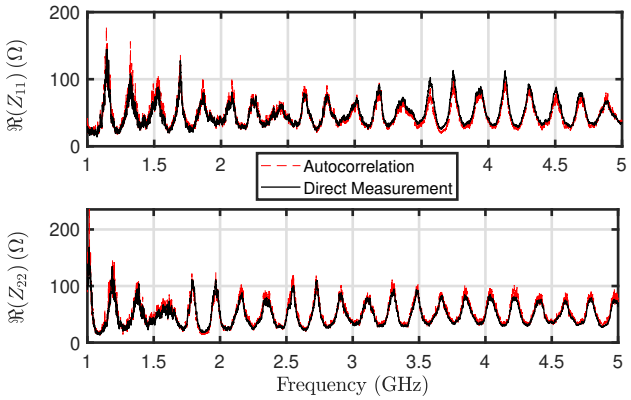

Fig. 6. Real parts of Z_{11} (above) and Z_{22} (below) obtained by a direct horn antenna measurement or through autocorrelation of Z_{iTx} impedances as a function of frequency.

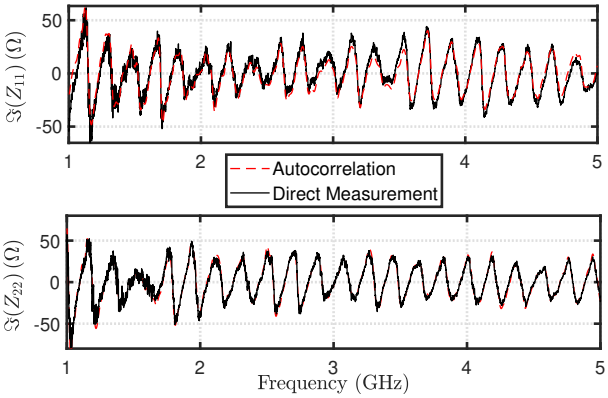

Fig. 9. Imaginary parts of Z_{11} (above) and Z_{22} (below) obtained by a direct horn antenna measurement or through autocorrelation of Z_{iTx} impedances as a function of frequency.

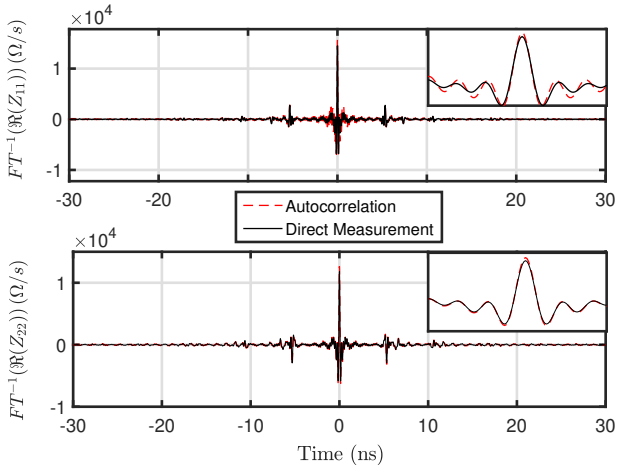

Fig. 7. Inverse Fourier transform of the real parts of Z_{11} (above) and Z_{22} (below) obtained by a direct horn antenna measurement or through autocorrelation of Z_{iTx} impedances as a function of time. Inset presents a zoom on the central peak.

impedance $Z_{12}^{causal}(t)$ is causal ($Z_{12}^{causal}(t) = 0$ for $t < 0$). The imaginary part of $Z_{12}(f)$ is then just the imaginary of the direct Fourier transform of $Z_{12}^{causal}(t)$. It is compared with the imaginary part of the directly measured impedance Z_{I12} in Fig. 8 and a good agreement is observed. A similar approach is applied to get the imaginary part of $Z_{11}(f)$ and $Z_{22}(f)$. However, contrary to $Z_{12}(t)$, $Z_{11}(t)$ or $Z_{22}(t)$ usually show a strong contribution near $t = 0$ that cannot be recovered just by using the folding technique. We empirically found that this effect can be mitigated by removing the frequency mean of the real part (respectively of $47.33\ \Omega$ for Z_{11} and $52.68\ \Omega$ for Z_{22}) that corresponds in the time domain to a Dirac pulse at $t = 0$. This operation is performed before the inverse Fourier transform and the time folding. The comparison in the frequency domain of the retrieved imaginary parts of Z_{11} and Z_{22} (that are Z_{I11}^{corr} and Z_{I22}^{corr}) with the ones obtained by the direct measurement (Z_{I11} and Z_{I22}) shows a good agreement (Fig. 9).

To quantify the agreement between the self and mutual impedances obtained by a direct measurement or through PSD or CSD, the Pearson's correlation coefficient is computed (see Tab. I) for the real and imaginary parts. The values between 0.927 and 0.995 confirm the good observed agreement.

TABLE I
PEARSON'S CORRELATION COEFFICIENTS COMPUTED BETWEEN REAL OR IMAGINARY PARTS OF IMPEDANCES OBTAINED BY A DIRECT MEASUREMENT AND THROUGH CORRELATION IN THE CASE OF THE TWO FACING HORN ANTENNAS.

	Pearson's correlation coefficients	
	Real	Imag
Z_{11}	0.995	0.937
Z_{22}	0.995	0.978
Z_{12}	0.927	0.950

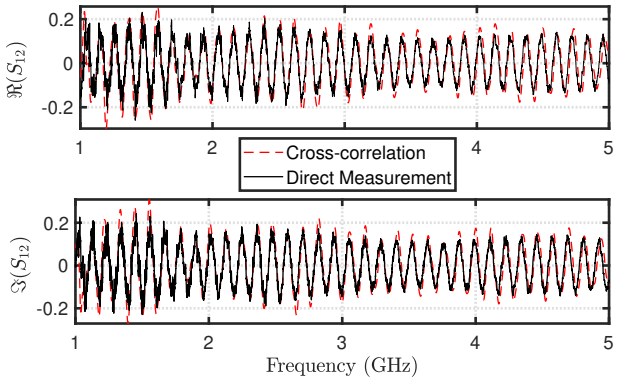

Fig. 10. Real part (above) and imaginary part (below) of S_{12} obtained by a direct horn antenna measurement or through PSD or CSD of impedances as a function of frequency.

C. Retrieval of the transmission coefficient

Once the 2×2 complex impedance matrix between antennas 1 and 2 is passively obtained, it is possible to reconstruct the transmission coefficient in the frequency domain from these impedances using the following formula :

$$S_{12}^{\text{rec}} = \frac{2Z_0 Z_{12}^{corr}}{(1+Z_{11}^{corr})(1+Z_{22}^{corr}) - Z_{12}^{corr}Z_{21}^{corr}} \tag{19}$$

where $Z_0 = 50\ \Omega$. The comparison in Fig. 10 of the reconstructed transmission coefficient with the one directly measured in Config$_{ref}$ validates this approach.

D. Results verification with a slot antenna

Whereas previous results were related to two facing directive antennas, an omnidirectional slot antenna, based on a half-disc slot excited by a microstrip [17], has then been placed in front of the horn antenna at a distance of 50 cm. As the bandwidth of the slot antenna is limited to 1.7GHz-2.8GHz, the measurement range is reduced to 1.4GHz-3.2GHz (20001 frequency points with an IF BW of 10 kHz). The same excitation antenna as well as source and stirrer positions as in the previous measurement have been used. Figs. 11 and 12 show a good agreement between the measured and reconstructed $\Re(Z_{12})$ impedances in the time as well as in the frequency domains, associated to a Pearson's correlation coefficient of 0.864.

IV. ANTENNA GAIN PATTERN ESTIMATION

The objective of this part is to estimate the gain pattern of an antenna in a totally passive way (AUTs only in reception)

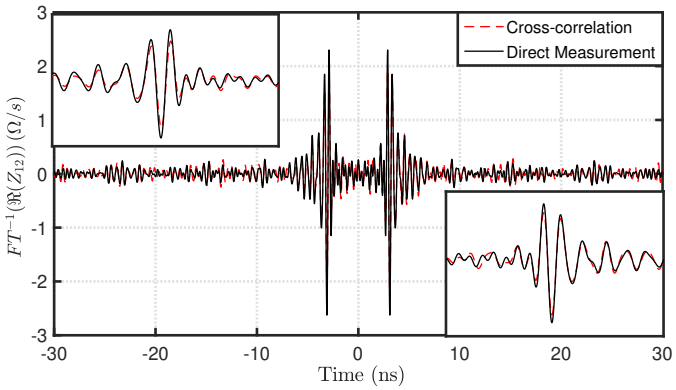

Fig. 11. Inverse Fourier Transform of the real part of Z_{12} obtained by a direct measurement between a horn antenna and a slot antenna or through CSD between impedances Z_{1Tx} and Z_{2Tx} as a function of time. Insets present zooms on the first peaks for negative and positive times.

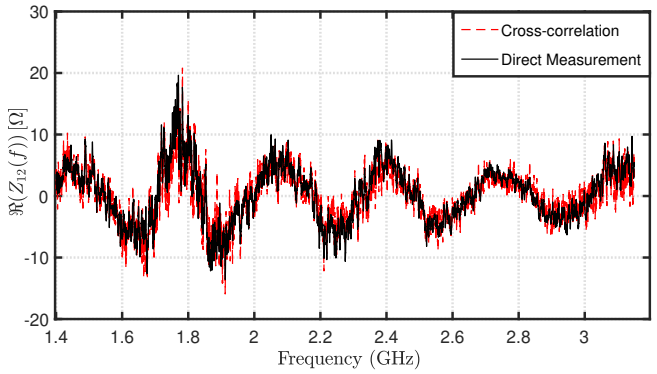

Fig. 12. Real part of Z_{12} obtained by a direct measurement between a horn antenna and a slot antenna or through through CSD between impedances Z_{1Tx} and Z_{2Tx} as a function of frequency.

exploiting the PSD and CSD technique. The approach is based on the theory developed in the first part of the paper and experimentally validated in the second part for two different horn antennas then a horn antenna and a printed one. The characterized antenna is the above-mentioned double-ridged horn antenna (A-INFO JXTXLB-10180). Measurements are performed with the same excitation horn antenna as in previous measurements (for $N_{src} = 11$ source positions and $N_{\text{mech}} = 60$ stirrer positions), and two identical double-ridged horn antennas facing each other and spaced at a distance of 109 cm. One of the AUTs is placed on a mast rotating from $\theta = -40°$ to $\theta = +40°$ with a rotation step of 2°. Thanks to the correlation technique, the 2×2 impedance matrix between both double-ridged horn antennas is passively retrieved at each position of the rotating AUT, and the transmission coefficient S_{21}^{rec} is reconstructed following the method presented in III-C. Antenna gain is then obtained from Friis formula using the modulus of the transmission coefficient.

The gain of the same antenna has then be characterized at 1.5 GHz and 2.5 GHz within an anechoic chamber for a distance between both facing antennas (the AUT and a MVG dual-ridge horn SH800) of 110 cm and for orientation angles of the AUT varying from $\theta = -40°$ to $\theta = +40°$ with a rotation step of 1°. It has to be noticed that the far-field

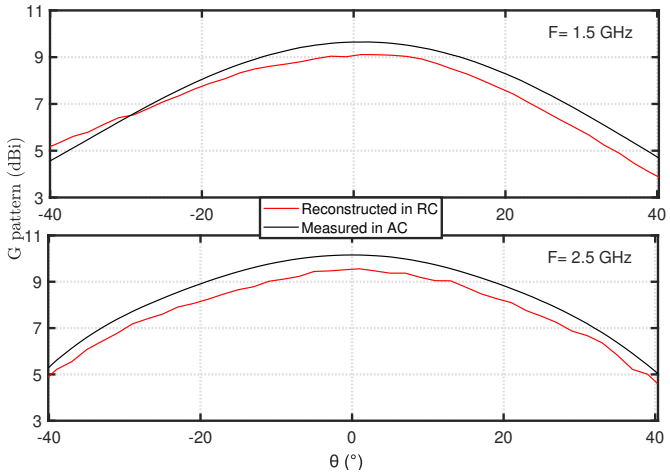

Fig. 13. Comparison of the gain patterns at 1.5 GHz and 2.5 GHz obtained through CSD in the RC with the ones measured classically in an anechoic chamber.

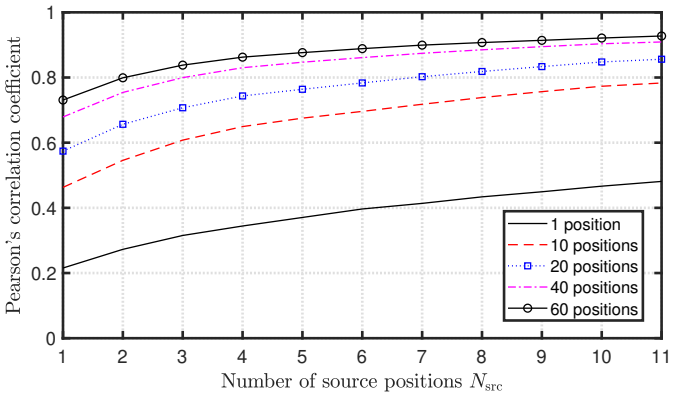

Fig. 14. 's correlation coefficient between the real part of Z_{12} obtained by a direct measurement or through correlations as a function of N_{src} and for various N_{mech}.

criterion is respected at 1.5GHz but not at 2.5GHz for this measurement distance. The comparison in Fig. 13 of the gain pattern of the double-ridge antenna extracted from passive measurements in the RC with the one obtained by the reference measurement in the anechoic chamber shows the possibility to extract passively antenna gain through the proposed CSD technique. The mean difference between both gain estimations over the angle range is of 0.465dB at 1.5 GHz and 0.597 dB at 2.5dB, and the difference between the maximal gain values are of 0.537dB at 1.5 GHz and 0.465 dB at 2.5 GHz.

V. Discussion

A. Stirring effect

The theory is based on the assumption of equipartitioned sources illuminating the AUTs. In our measurement setup, this condition is approached while varying the cavity configuration through the rotation of the mechanical stirrer ($N_{mech} = 60$) and of the excitation antenna ($N_{src} = 11$), leading to 660 measurement configurations. The field generated within an RC by a single excitation antenna is assumed to be statistically uniform, isotropic and depolarized; the multitude of noise sources required by the correlation technique is thus replaced by an ensemble of diffuse field distributions associated to different RC configurations. To evaluate the RC performances in the considered measurement conditions, the number of uncorrelated configurations has been estimated using the methodology presented in [18]. We found that there are 49 uncorrelated stirrer positions out of 60 and 7 uncorrelated source orientations out of 11. The resulting total number of uncorrelated RC configurations is thus estimated to $49 \times 11 = 539$.

To highlight the role of both stirring processes on the convergence of the measured correlation towards the theoretical one, the Pearson's correlation coefficient between the real parts of Z_{12} directly measured or estimated through correlation is computed as a function of the number of source positions N_{src} for various angular positions of the mechanical stirring N_{mech}. Results are presented in Fig. 14. As expected, the more configurations, the higher the Pearson's coefficient. When only one configuration is considered, i.e., $N_{\text{src}} = 1$ and $N_{\text{mech}} = 1$, the Pearson's coefficient is equal to only 0.215. Also, it confirms that the source stirring is as efficient as the mechanical stirrer to provide uncorrelated configurations. Indeed, the case $N_{\text{src}} = 1$ and $N_{\text{mech}} = 10$ leads to almost the same Pearson's coefficient as the case $N_{\text{src}} = 10$ and $N_{\text{mech}} = 1$, i.e, about 0.465.

B. Impact of antenna location and properties

The accuracy of the impedance reconstruction has been quantified through the Pearson's correlation coefficient. In this part, we compare the Pearson's coefficients obtained for different AUT positions or properties while considering all mechanical stirrer and excitation antenna positions (i.e. 660 measurement configurations).

First measurements were performed for a distance d between both AUTs equals to 50 cm, with, in the first case, two horn antennas (Section III-B), and in the second case a horn antenna and an omnidirectional slot antenna (Section III-D). In both cases, the AUTs are facing each other to maximize the transmission between them. The Pearson's correlation coefficient between measured and reconstructed $\Re(Z_{12})$ is of 0.927 in the first case. In the second case, the coefficient decreases to 0.864. This lower value can be explained by the lower amplitude of $\Re(Z_{12})$, resulting in a lower signal-to-noise ratio. Indeed, the maximum value of $\Re(Z_{12}(t))$ is of 1164 Ω/s between the two horn antennas while it is only 2.62 Ω/s between the slot antenna and the horn antenna.

We now consider the results with two horn antennas at a distance d of 109 cm from each other. One of the 2 antennas (Section IV) is fixed on a stepper motor rotation stage. The variation of the Pearson's coefficient versus the angle between the axes of the 2 horn antennas is shown in Fig. 15. We first notice that because of the lower coupling level between antennas when $d = 109$, the maximal Pearson's coefficient value obtained for $\theta \approx 0°$ is 0.877 instead of 0.927 when $d = 50$ cm. For the same coupling reason, the larger the angle and the smaller the Pearson's coefficient. Note that the asymmetry of this figure with respect to the angle can

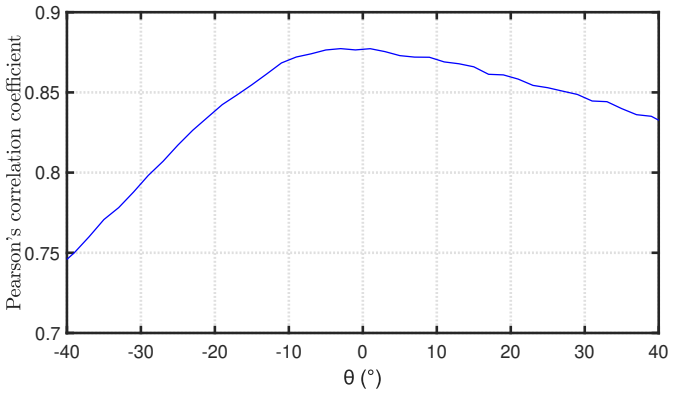

Fig. 15. Pearson's correlation coefficient between the real part of Z_{12} obtained by a direct measurement or through correlations as a function of AUT angular position in the antenna gain pattern estimation measurement.

be explained by an imperfect alignment between AUTs and the fact that the level of fluctuations may also be slightly anisotropic.

C. Measurements with open-circuits

As presented in the setup of the first measurement configuration, both switches permit to connect the AUTs alternatively to the VNA or an open-circuit load. The choice of this load is in agreement with the definition of the impedances. Indeed, by definition, the impedance Z_{ij} is the ratio of the voltage measured on port i and the current on port j when all the currents on the other ports ($i \neq j$) are 0. Therefore, when AUT1 is connected to the VNA and AUT2 to an open-circuit (Config_1), the measured S-parameters lead to the knowledge of the impedances Z_{11}, Z_{1Tx} and Z_{TxTx}, whereas the complementary configuration Config_2 (AUT1 connected to the open-circuit and AUT2 to the VNA) leads to Z_{22}, Z_{2Tx} and Z_{TxTx}. However, in measurement an open-circuit is never ideal, in particular on a large frequency band. To verify the accuracy of this approach, the real part of Z_{12} impedance retrieved by CSD after this two-step measurement has been compared to the one issued from the CSD of impedances obtained by the direct measurement in Config_{ref} of the 3×3 S-matrix between the three antennas (the excitation antenna and both AUTs). The obtained similarity coefficient of 0.9997 permits to validate this approach consisting of using open-circuit loads.

Once the proposed measurement approach is validated, that could be used to perform passive measurements, the following measurements (with the slot antenna then for the gain pattern) have been performed while directly connecting the three antennas to the VNA (without switches), in order to accelerate the measurement process.

VI. Conclusion

In this paper, we have presented a passive measurement technique to estimate the 2×2 impedance matrix between two receiving antennas. As the underlying theory leans on the assumption of uniformly distributed sources, measurements have been performed within an RC excited by a single source where mechanical and source stirring techniques have been combined to enhance the number of measurement configurations. For the first time, explicit formulas have been derived from a theoretical approach linking, in the diffuse field environment generated within an RC, the real parts of self and mutual impedances of two coupled antennas in receiving mode with the power and cross spectral densities of impedances weighted by measurement setup properties. Our model includes losses within the cavity as well as excitation and reception antenna losses. The exposed theoretical developments have been experimentally validated while considering antennas of different properties, and it has been proven that, besides the retrieval of the real parts of the impedances, it is possible to reconstruct the complex impedance matrix as well as the transmission coefficient between both receiving antennas. Once the impedance matrix and the transmission coefficient are obtained, the presented correlation method offers the potential to characterize more extensively antennas or antenna arrays, as shown with the extraction of the gain pattern of a horn antenna that is achieved with a good accuracy.

The presented approach paves the way to characterization of antennas that cannot be turned into emitting modes, as small embedded antennas. Moreover, even if we only considered two receiving antennas in this paper, this passive antenna characterization technique can be extended to a higher number of receiving antennas, and it could permit to accelerate the characterization of the mutual coupling matrix of large antenna arrays: indeed, the mutual coupling between each pair of antennas could be done without turning antennas successively in their emitting and receiving modes but while keeping all array antennas in their receiving mode and using another antenna to generate the required diffuse field. The condition is that each antenna port can be set to a high impedance level. Besides, the possible use of cross-correlation techniques for passive imaging applications has already been demonstrated in several physics domains [4] [7]. The sensitivity of the proposed approach to a geometrical parameter variation has been shown with the reconstruction of the antenna gain pattern obtained while rotating the AUT; it is thus promising to detect environment variations in a passive imaging context.

Acknowledgements

The authors acknowledge funding from the French "Agence Nationale de la Recherche" under reference ANR-17-ASTR-0017.

References

[1] R. L. Weaver and O. I. Lobkis, "Ultrasonics without a source: Thermal fluctuation correlations at mhz frequencies," *Physical Review Letters*, vol. 87, p. 044204134301, 2001.

[2] O. I. Lobkis and R. L. Weaver, "On the emergence of the green's function in the correlations of a diffuse field," *The Journal of the Acoustical Society of America*, vol. 110, p. 3011, 2001. [Online]. Available: 10.1121/1.1417528

[3] M. Campillo and A. Paul, "Long-range correlations in the diffuse seismic coda," *Science*, vol. 299, pp. 547–549, 2003.

[4] L. Chehami, E. Moulin, J. de Rosny, C. Prada, O. Bou Matar, F. Benmeddour, and J. Assaad, "Detection and localization of a defect in a reverberant plate using acoustic field correlation," *J. Appl. Phys.*, vol. 115, p. 104901, 2014.

[5] C. Hadziioannou, E. Larose, O. Coutant, P. Roux, and M. Campillo, "Stability of monitoring weak changes in multiply scattering media with ambient noise correlation: Laboratory experiments," *The Journal of the Acoustical Society of America*, vol. 125, p. 3688, 2009.

[6] T. Nowakowski, L. Daudet, and J. de Rosny, "Localization of acoustic sensors from passive green's function estimation," *The Journal of the Acoustical Society of America*, vol. 138, p. 3010, 2015.

[7] M. Davy, M. Fink, and J. de Rosny, "Green's function retrieval and passive imaging from correlations of wideband thermal radiations," *Physical Review Letters*, vol. 110, p. 203901, 2013.

[8] M. Davy, J. de Rosny, and P. Besnier, "Green's function retrieval with absorbing probes in reverberating cavities," *Physical Review Letters*, vol. 116, p. 213902, 2016.

[9] P. del Hougne, J. Sol, F. Mortessagne, P. Besnier, and M. Davy, "Diffuse field cross-correlation in a programmable-metasurface-stirred reverberation chamber," *Appl. Phys. Lett.*, vol. 118, p. 104101, 2021. [Online]. Available: https://doi.org/10.1063/5.0039596

[10] R. H. Dicke, "The measurement of thermal radiation at microwave frequencies," *Review of Scientific Instruments*, vol. 17, no. 7, pp. 268–275, 1946. [Online]. Available: https://doi.org/10.1063/1.1770483

[11] S. Rytov, A. Repyev, Y. Kravtsov, and V. Tatarskii, *Principles of Statistical Radiophysics 3: Elements of Random Fields*. Springer Berlin Heidelberg, 1989.

[12] R. Twiss, "Nyquist's and thevenin's theorems generalized for nonreciprocal linear networks," *Journal of Applied Physics*, vol. 26, pp. 599–602, 1955. [Online]. Available: https://doi.org/10.1063/1.1722048

[13] M. Davy, P. Besnier, P. del Hougne, J. de Rosny, E. Richalot, F. Sarrazin, D. V. Savin, F. Mortessagne, U. Kuhl, and O. Legrand, "Diffuse field cross-correlations: Scattering theory and electromagnetic experiments," *Phys. Rev. E*, vol. 104, p. 044204, Oct 2021. [Online]. Available: https://link.aps.org/doi/10.1103/PhysRevE.104.044204

[14] M. Tamart, F. Sarrazin, E. Richalot, M. Davy, and J. de Rosny, "Diffuse field cross-correlation in a reverberantion chamber," in *IEEE Int. Symp. Antennas Propag. Soc.*, 2020, pp. 1179–1180.

[15] H. Haus and R. Adler, *Circuit Theory of Linear Noisy Networks*. MIT Press, 1959.

[16] D. Hill, "Electromagnetic theory of reverberation chambers," 1998-12-01 1998.

[17] W. Krouka, F. Sarrazin, J. Sol, P. Besnier, and E. Richalot, "Biased estimation of antenna radiation efficiency within reverberation chambers due to unstirred field: Role of antenna stirring," *IEEE Transactions on Antennas and Propagation*, 2022.

[18] C. Lemoine, P. Besnier, and M. Drissi, "Estimating the effective sample size to select independent measurements in a reverberation chamber," *IEEE Transactions on Electromagnetic Compatibility*, vol. 50, pp. 227–236, May 2008.